Frequency damage indicators for piezoelectric composites

*Ayech Benjeddou[1], Mohsen Hamdi[2] and Samir Ghanmi[3]

[1] *Structures, SUPMECA, Saint Ouen 93400, France*
[1] *benjeddou@supmeca.fr*
[2,3] *Technology department, IPEIN, Nabeul 8000, Tunisia*

ABSTRACT

The present contribution focuses on vibration-based damage detection of laminated composite beams using integrated piezoceramic patches and frequency indicators. The latter are assessed via three-dimensional fully coupled piezoelectric finite element parametric analyses on the damage key parameters under different mechanical and electrical conditions, and for all types of vibration modes. It is found that *squared* frequency change factors' performances are much better, as damage indicators, than simple frequency change ones; moreover, open-circuit frequency–based damage indicators' performances are found to be similar to short-circuit ones. The obtained results can be further used, for example, for training artificial neural networks for the quantification of the analyzed damage types (crack and delamination).

1. INTRODUCTION

Vibration-based damage detection (VBDD) for structural health monitoring (SHM) is a well-established technique for passive (Sinou 2009) and active (Huang *et al.* 2010) structures. However, except few works (Jian *et al.* 1997, Penn *et al.* 1999, Tan and Tong 2004, Yam *et al.* 2004, Benjeddou 2006, Benjeddou *et al.* 2006, Qiao *et al.* 2007, Al-Ajmi and Benjeddou 2008), the use of piezoceramic transducers as sensors or/and actuators was mainly limited to Lamb waves (see for example Ihn *et al.* 2008)- and impedance (see for example Giurgiutiu *et al.* 2011)–based high frequency approaches. It is then the objective of the present contribution to focus on low-frequency VBDD for piezoelectric laminated composite beams. Hence, frequency damage indicators, other than the classical simple frequency change (Tan and Tong 2004), are here explored via parametric analyses on the damage key parameters (position, length, depth) and on various mechanical (clamped-free, CF; clamped–supported, CS; clamped-clamped, CC; supported–supported, SS) and electrical (short–circuit, SC; open–circuit, OC)

---

[1] Full Professor
[2] PhD Student
[3] Assistant Professor

conditions. For this purpose, three-dimensional (3D) piezoelectric fully coupled finite element (FE) analyses are used for assessing the effects of these parameters and conditions on the proposed VBDD indicators performance for all types of vibration modes (bending, membrane and torsion). The damage is modeled as a *removal of material* (RM), simulating a *crack* (Qiao *et al.* 2007), and as *inclusion of a soft layer* (ISL) of Teflon[®] material, simulating a *delamination* (Yam *et al.* 2004).

The added values of the present work to the authors' earlier ones and to the current state of the art of VBDD of composite structures with piezoelectric patches are: (i) use of 3D fully coupled piezoelectric FE models instead of one-dimensional (1D) models that do not model explicitly the beam width; (ii) considering all mode types (bending, membrane and torsion) instead of transverse bending ones only as previously retained; (iii) considering most mechanical boundary conditions (BC) and not only the popular CF or SS ones; (iv) investigation of a new OC frequency-based damage indicator;

Hence, hereafter, frequency damage indicators are first discussed; then, simple and squared frequency-change factor (FCF) indicators are analyzed first under fixed RM and ISL damage characteristics; next, they are assessed through FE parametric analyses under RM and ISL varied damage characteristics of hybrid carbon/graphite fiber reinforced polymer (CFRP/GFRP) composite laminated beams with symmetrically integrated pair of piezoceramic (PZT-5A) patches under four (CF, CS, CC, SS) mechanical and two (SC, OC) electrical conditions. Finally, conclusions and perspectives are given as a closure.

2. FREQUENCY-BASED DAMAGE INDICATORS

A *qualitative* way to track damage presence in a structure is to compare tabulated damage frequencies (f_d) to healthy ones (f_h) of the vibrating structure as considered in Penn *et al.* (1999) for controlled delaminated (created by placing inter-ply Teflon[®] polyimide release film pieces) unidirectional (UD) GFRP cantilever plates using piezoelectric polymer (PVDF) sensors.

A *quantitative* detection was considered earlier, in Jian *et al.* (1997), through graphical representations, versus mode number, of this *frequencies ratio* (*FR*) indicator

$$FR = \frac{f_d}{f_h} \qquad (1)$$

It's worthy to notice that in these experimental analyses (Jian *et al.* 1997, Penn *et al.* 1999) no indication was given on the electric conditions (SC or OC) applied to the electrodes of piezoelectric sensors bonded to the vibrating composite plates.

Later, in Tan and Tong (2004), the following percent *frequencies change (FC)* was used for delamination detection of composite beams using piezoceramic (PZT) sensors

$$FC \ (\%) = 100 \times \frac{f_d - f_h}{f_h} = 100 \times (\frac{f_d}{f_h} - 1) \qquad (2)$$

Here (Tan and Tong 2004) also, no indication was given on the electric conditions applied to the electrodes strips made on the piezoelectric sensors surfaces.

First consideration of the electric conditions applied on the electrodes of the piezoelectric actuators or sensors was proposed by Benjeddou et al. (2006), for piezoelectric hybrid CFRP/GFRP laminated composite cantilever beams, through this percent *frequency change factor* (*FCF*) that uses damaged and healthy frequencies under SC patches' electrodes

$$FCF_{sc} \ (\%) = 100 \times \frac{(f_{sc})_h - (f_{sc})_d}{(f_{sc})_h} = 100 \times (1 - FR_{sc}) \tag{3}$$

Notice in eq. (3) the opposite sign to Eq. (2); it is motivated by the fact that the damage generally reduces the frequencies (Yam *et al.*, 2004); hence this definition is expected to provide mostly positive values of the damage presence indicator.

A new OC FCF damage indicator is here proposed in order to investigate the piezoelectric effect (present under OC conditions) influence on the simple FCF

$$FCF_{oc} \ (\%) = 100 \times \frac{(f_{oc})_h - (f_{oc})_d}{(f_{oc})_h} = 100 \times (1 - FR_{oc}) \tag{4}$$

This indicator is to be compared to above SC FCF one, as given in Eq. (3), that inherently does not show the piezoelectric effect.

Later, in Al-Ajmi and Benjeddou (2008), new indicators using *squared* frequencies under SC and OC patches' electrodes were proposed as follows, respectively

$$FCF_{sc}^2 \ (\%) = 100 \times \frac{(f_{sc}^2)_h - (f_{sc}^2)_d}{(f_{sc}^2)_h} = 100 \times (1 - FR_{sc}^2) \tag{5}$$

$$FCF_{oc}^2 \ (\%) = 100 \times \frac{(f_{oc}^2)_h - (f_{oc}^2)_d}{(f_{oc}^2)_h} == 100 \times (1 - FR_{oc}^2) \tag{6}$$

The last four VBDD indicators, as defined in Eq. (3) – Eq. (6), will be assessed on the same piezoelectric hybrid laminated composite beam benchmark, but under various mechanical and electrical BC. Also, all mode types will be considered thanks to the use of a 3D fully coupled piezoelectric FE model with the help of ANSYS® commercial code.

3. DAMAGE INFLUENCE ON MODAL PROPERTIES AND INDICATORS

The benchmark used for the assessment of above frequency-based damage indicators is that proposed in Benjeddou *et al.* (2006); it consists of a 32-ply symmetric laminated composite beam with dimensions $L \times B \times H = 200 \times 20 \times 4$ mm^3 and symmetric stacking sequence of [$\mathbf{0}_4$/90$_8$/0$_4$]$_S$, where bold plies are made of GFRP, while the others are in CFRP. Two piezoceramic (PZT-5A) patches, polarized along their thickness and of dimensions $L_a \times B \times H_a = 25 \times 20 \times 0.5$ mm^3, are placed in replacement of bottom and top four 90°-plies at the length position of $X_a = 22.5$ mm from the beam left end. The sketched geometrical model shown in Fig. 1 is meshed using 3D quadratic (20 nodes) elastic (displacement) SOLID191 and fully coupled piezoelectric SOLID226

(displacement-potential) FE for composite and piezoelectric layers, respectively, according to the subdivisions summarized in Table 1; this leads to a FE mesh of 4480 elements and 21879 nodes. Materials data are given in Appendix A. The geometric and FE model are shown in Fig. 2.
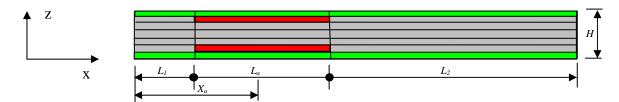

Fig. 1 Smart hybrid laminated beam sketch (red: PZT-5A, green: GFRP, gray: CFRP)

Table 1 3D FE discretization of the smart hybrid healthy laminate composite beam

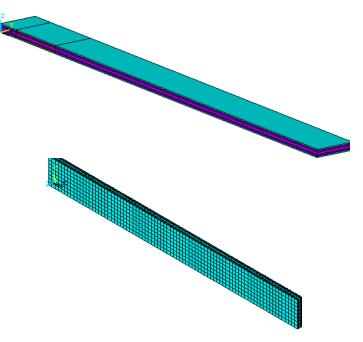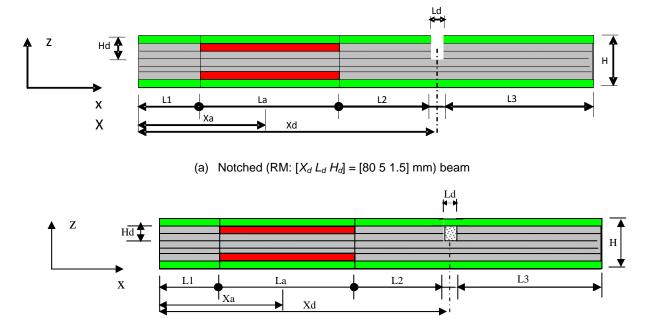| Healthy beam	Geometric parameter	Dimension (mm)	Number of elements	Size of elements (mm)
Host composite	L_1	10	4	2.5
	L_a	25	10	2.5
	L_2	165	66	2.5
	B	20	8	2.5
	H	4	1	1
PZT	L_a	25	10	2.5
	B_a	20	8	2.5
	Hp	0.5	1	0.5

Fig. 2 Smart hybrid laminated composite beam (a) geometric and (b) FE 3D models

Two types of damages are considered; the first simulates a notch or crack, and is modeled by the removal of corresponding material, while the second simulates a

delamination and is modeled by an inclusion of a soft layer made of a thin Teflon® film. The corresponding geometrical sketches are shown in Fig. 3, while their FE mesh details are provided in Table 2, leading to 4432 elements and 21747 nodes for the RM model, and 4480 elements and 21879 nodes for the ISL one; they are shown in Fig. 4.

(a) Notched (RM: $[X_d\ L_d\ H_d]$ = [80 5 1.5] mm) beam

(b) Delaminated (ISL: $[X_d\ L_d\ H_d]$ = [80 5 1] mm) beam

Fig. 3 Damaged hybrid composite beam (red: PZT-5A, green: GFRP, gray: CFRP)

Table 2 3D FE discretization of the *damaged* smart hybrid composite beam

Damaged beam	Geometric parameter	Dimension (mm)	Number of elements	Size of elements (mm)
Host composite	L_1	10	4	2.5
	L_a	25	10	2.5
	L_2	42.5	17	2.5
	L_3	117.5	47	2.5
	B	20	8	2.5
	H	4	1	0.5, 1
PZT	L_a	25	10	2.5
	B_a	20	8	2.5
	Hp	0.5	1	0.5
Notched (RM) damage	L_d	5	2	2.5
	B_d	20	8	2.5
	H_d	1.5	3	0.5
Delamination (ISL) damage	L_d	5	2	2.5
	B_d	20	8	2.5
	H_d	1	2	0.5

(a) RM 3D geometric model

(b) RM 3D FE model

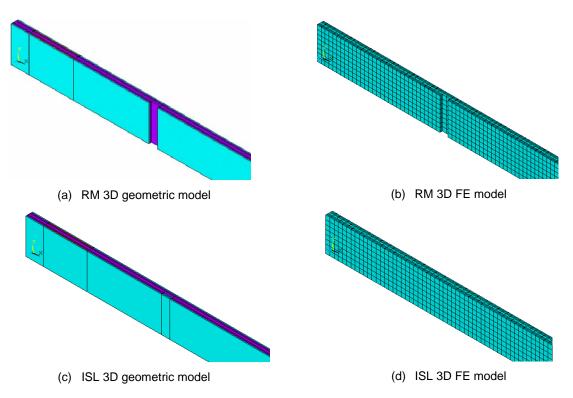(c) ISL 3D geometric model

(d) ISL 3D FE model

Fig. 4 Damaged hybrid composite beam (a,c) geometric and (b,d) FE 3D models

The FE simulations have been conducted for the healthy and damage (RM and ISL) smart hybrid laminated composite beam under four mechanical BC (CF, CS, CC, SS) and two electric conditions (SC, OC). The obtained results are shown in Table 3, where bold values indicate electromechanically uncoupled modes since there is no difference between SC and OC values (tenth or hundredth Hz differences are only numerical). Worthy to mention that clamping is obtained by fixing the FE three displacements (translations) degrees of freedom (DOF) to zero values, while simply-supported condition is modeled here by letting free only the axial displacement (translation) DOF. From the results, it can be observed that (i) only the RM damage changes the modes types for only the CF BC; (ii) the modes' electromechanical coupling is not affected by the damage since the healthy uncoupled x-y in-plane bending and torsion modes remain uncoupled for the damaged (RM and ISL) beams; hence, only the transverse (x-z) bending modes are coupled and affected by the damage; (iii) in contrary to the RM damage model, the ISL one does not affect the mode order and type; care should be then taken when using RM model for the damage simulation under CF BC since it affects the modes types and order (see modes 2, 3, 7, 8 of this case); (iv) the CS, CC and SS BC have different modes' types than the CF one; besides, the SS BC case has different 3rd and 4th modes' types than CS and CC BC which have the same modes' types; hence, it appears clearly that the popular numerical CF and analytical SS BC are not the best ones for studying theoretically (numerically or analytically) the VBDD performance in 3D modeling which is the realistic way of simulating actual damaged structures which have intrinsically a 3D response; the best BC from this point of view are then CS and CC, with a preference to the latter due to its practical interest.

1055

Table 3 First 8 *frequencies* (Hz) of healthy and damaged smart hybrid composite beams

BC	Mode order	Healthy frequencies (Hz)			RM frequencies (Hz)			ISL frequencies (Hz)		
		Type	SC	OC	Type	SC	OC	Type	SC	OC
CF	1	f_{xz}^1	95.264	96.048	f_{xz}^1	92.711	93.429	f_{xz}^1	95.793	96.456
	2	f_{xy}^1	**574.05**	**574.06**	f_{xz}^2	560.41	562.20	f_{xy}^1	**580.25**	**580.25**
	3	f_{xz}^2	576.25	577.84	f_{xy}^1	**570.93**	**570.94**	f_{xz}^2	580.41	581.79
	4	t^1	**841.67**	**841.67**	t^1	820.15	820.16	t^1	**839.14**	**839.14**
	5	f_{xz}^3	1555.6	1555.9	f_{xz}^3	1531.5	1531.9	f_{xz}^3	1560.3	1560.6
	6	t^2	**2530.2**	**2530.2**	t^2	**2548.0**	**2548.0**	t^2	**2546.8**	**2546.8**
	7	f_{xy}^2	**2901.7**	**2901.7**	f_{xz}^4	**2894.3**	**2896.4**	f_{xy}^2	**2924.5**	**2924.5**
	8	f_{xz}^4	2934.5	2936.4	f_{xy}^2	2904.6	2904.6	f_{xz}^4	2941.5	2943.2
CS	1	f_{xz}^1	406.49	408.09	f_{xz}^1	402.72	404.45	f_{xz}^1	409.28	410.65
	2	f_{xz}^2	1270.2	1271	f_{xz}^2	1235.8	1236.6	f_{xz}^2	1277.0	1277.6
	3	t^1	**1668.8**	**1668.8**	t^1	**1664.4**	**1664.4**	t^1	**1674.7**	**1674.7**
	4	f_{xy}^1	**2088.9**	**2088.9**	f_{xy}^1	**2089.9**	**2089.9**	f_{xy}^1	**2104.3**	**2104.3**
	5	f_{xz}^3	2547	2547.7	f_{xz}^3	2536.2	2537.0	f_{xz}^3	2548.4	2549.1
	6	t^2	**3353.7**	**3353.7**	t^2	**3330.2**	**3330.2**	t^2	**3360.8**	**3360.8**
	7	f_{xz}^4	4219.5	4227.9	f_{xz}^4	4080.7	4088.3	f_{xz}^4	4249.7	4257.1
	8	t^3	**5028.6**	**5028.7**	t^3	**4937.6**	**4937.6**	t^3	**5021.1**	**5021.2**
CC	1	f_{xz}^1	584.2	585.91	f_{xz}^1	573.99	575.87	f_{xz}^1	589.01	590.48
	2	f_{xz}^2	1548.4	1548.7	f_{xz}^2	1522.8	1523.1	f_{xz}^2	1552.9	1553.2
	3	t^1	**1777.8**	**1777.8**	t^1	**1778.0**	**1778.0**	t^1	**1785.9**	**1785.9**
	4	f_{xy}^1	**2666.7**	**2666.7**	f_{xy}^1	**2677.6**	**2677.6**	f_{xy}^1	**2689.2**	**2689.2**
	5	f_{xz}^3	2917.1	2919	f_{xz}^3	2879.0	2881.0	f_{xz}^3	2923.7	2925.3
	6	t^2	**3544.3**	**3544.4**	t^2	**3499.1**	**3499.1**	t^2	**3545.8**	**3545.9**
	7	f_{xz}^4	4685.1	4696.1	f_{xz}^4	4558.9	4568.3	f_{xz}^4	4715.2	4725.0
	8	t^3	**5288.2**	**5288.3**	t^3	**5208.1**	**5208.2**	t^3	**5288.0**	**5288.1**
SS	1	f_{xz}^1	253.92	254.1	f_{xz}^1	242.78	242.93	f_{xz}^1	255.31	255.46
	2	f_{xz}^2	988.59	991.32	f_{xz}^2	974.80	977.20	f_{xz}^2	992.04	994.34
	3	f_{xy}^1	**1470.6**	**1470.6**	f_{xy}^1	**1470.2**	**1470.2**	f_{xy}^1	**1480.2**	**1480.2**
	4	t^1	**1587.7**	**1587.7**	t^1	**1588.5**	**1588.5**	t^1	**1595.0**	**1595.0**
	5	f_{xz}^3	2171.5	2181.8	f_{xz}^3	2133.2	2144.4	f_{xz}^3	2184.3	2192.9
	6	t^2	**3088.8**	**3088.9**	t^2	**3038.0**	**3038.0**	t^2	**3087.9**	**3087.9**
	7	f_{xz}^4	3808.4	3827.6	f_{xz}^4	3705.2	3722.1	f_{xz}^4	3838.5	3855.4
	8	t^3	**4558.4**	**4558.4**	t^3	**4495.5**	**4495.5**	t^3	**4570.2**	**4570.3**

Processing SC and OC frequency results of Table 3 provides SC and OC FCF (Eqs. 3 and 4) and squared FCF (Eqs. 5 and 6) ones given in Table 4. The latter indicates for FCF indicators that: (i) due to the more structural degradation, RM indicators have much higher values than ISL ones, although both of them remain low (less than 5%); (ii) RM indicators are mostly positive, while ISL ones are mostly negative, indicating that in contrary to the RM damage which decreases the healthy frequencies (see Eq. 3), the ISL damage increases the healthy frequencies (Eq. 4); (iii) OC and SC indicators

highest values (in bold) are obtained for transverse bending modes under all BC for RM damage, but for the first membrane mode for the ISL damage under all BC, except the SS case; (iv) SC and OC FCF maximum values can be different for the RM damage model but are the same for the ISL one.

Table 4 First 8 modes *FCF damage indicators* (%) of the smart hybrid composite beams

Damage model		RM				ISL			
	Mode	FCF (%)		Squared FCF (%)		FCF (%)		Squared FCF (%)	
BC	type	SC	OC	SC	OC	SC	OC	SC	OC
CF	f_{xz}^1	2.68	**2.73**	5.29	**5.38**	-0.55	-0.42	-1.11	-0.85
	f_{xy}^1	0.54	0.54	1.08	1.08	**-1.08**	**-1.08**	**-2.17**	**-2.17**
	f_{xz}^2	**2.75**	2.71	**5.42**	5.34	-0.72	-0.68	-1.45	-1.37
	t^1	2.56	2.55	5.05	5.04	0.30	0.30	0.60	0.60
	f_{xz}^3	1.55	1.54	3.07	3.06	-0.30	-0.30	-0.60	-0.60
	t^2	-0.70	-0.70	-1.41	-1.41	-0.66	-0.66	-1.32	-1.32
	f_{xy}^2	-0.10	-0.10	-0.20	-0.20	-0.78	-0.78	-1.58	-1.58
	f_{xz}^4	1.37	1.36	2.72	2.70	-0.24	-0.23	-0.48	-0.46
CS	f_{xz}^1	0.93	0.89	1.85	1.77	-0.69	-0.63	-1.38	-1.26
	f_{xz}^2	2.71	2.71	5.34	5.34	-0.53	-0.52	-1.07	-1.04
	t^1	0.26	0.26	0.53	0.53	-0.35	-0.35	-0.71	-0.71
	f_{xy}^1	-0.05	-0.05	-0.09	-0.09	**-0.74**	**-0.74**	**-1.48**	**-1.48**
	f_{xz}^3	0.42	0.42	0.85	0.84	-0.05	-0.05	-0.11	-0.11
	t^2	0.70	0.70	1.40	1.40	-0.21	-0.21	-0.42	-0.42
	f_{xz}^4	**3.29**	**3.30**	**6.47**	**6.49**	-0.71	-0.69	-1.44	-1.39
	t^3	1.81	1.81	3.59	3.59	0.15	0.15	0.30	0.30
CC	f_{xz}^1	1.75	1.71	3.46	3.40	-0.82	-0.78	-1.65	-1.57
	f_{xz}^2	1.65	1.65	3.28	3.28	-0.29	-0.29	-0.58	-0.58
	t^1	-0.01	-0.01	-0.02	-0.02	-0.45	-0.45	-0.91	-0.91
	f_{xy}^1	-0.41	-0.41	-0.82	-0.82	**-0.84**	**-0.84**	**-1.69**	**-1.69**
	f_{xz}^3	1.31	1.30	2.59	2.59	-0.23	-0.21	-0.45	-0.43
	t^2	1.27	1.28	2.53	2.54	-0.04	-0.04	-0.08	-0.08
	f_{xz}^4	**2.69**	**2.72**	**5.31**	**5.37**	-0.64	-0.61	-1.29	-1.23
	t^3	1.51	1.51	3.01	3.01	0.00	0.00	0.01	0.01
SS	f_{xz}^1	**4.39**	**4.39**	**8.58**	**8.60**	-0.55	-0.53	-1.10	-1.07
	f_{xz}^2	1.39	1.42	2.77	2.83	-0.35	-0.30	-0.70	-0.61
	f_{xy}^1	0.03	0.03	0.05	0.05	-0.65	-0.65	-1.31	-1.31
	t^1	-0.05	-0.05	-0.10	-0.10	-0.46	-0.46	-0.92	-0.92
	f_{xz}^3	1.76	1.71	3.50	3.40	-0.59	-0.51	-1.18	-1.02
	t^2	1.64	1.65	3.26	3.27	0.03	0.03	0.06	0.06
	f_{xz}^4	2.71	2.76	5.35	5.44	**-0.79**	**-0.73**	**-1.59**	**-1.46**
	t^3	1.38	1.38	2.74	2.74	-0.26	-0.26	-0.52	-0.52

For the squared FCF, it is found that these indicators are much more performant (having much higher values) for indicating both RM and ISL damages than the FCF

ones; they are then retained for the subsequent parametric analyses; therefore, since SC and OC values are found to be close to each other, focus is made mainly on SC squared FCF in order to get reference with earlier 1D results (Benjeddou *et al.* 2006).

3. DAMAGE DETECTION INDICATORS PARAMETRIC ASSESMENT

In order to check the validity of above obtained results for fixed MR and ISL damage characteristics of $[X_d\ L_d\ H_d]$ = [80 5 1.5] mm and [80 5 1] mm, respectively, these parameters are varied according to the values summarized in Table 5.

Table 5 Damage characteristics variations for the parametric analysis of damaged smart hybrid composite beams

Model	parameters case	X_d (mm) X_d/L						L_d (mm) L_d/L				H_d (mm) H_d/H		
RM	1	60 *0.3*						5 *0.025*	10 *0.05*	15 *0.075*	20 *0.1*	0.5 *0.0125*	1 *0.25*	1.5 *0.375*
	2	60 *0.3*	80 *0.4*	100 *0.5*	120 *0.6*	140 *0.7*	160 *0.8*	5 *0.025*				0.5 *0.0125*	1 *0.25*	1.5 *0.375*
	3	60 *0.3*	80 *0.4*	100 *0.5*	120 *0.6*	140 *0.7*	160 *0.8*	5 *0.025*	10 *0.05*	15 *0.075*	20 *0.1*	1.5 *0.375*		
ISL	1	60 (fixed) *0.3*						5 *0.025*	10 *0.05*	15 *0.075*	20 *0.1*	0.5 *0.0125*	1 *0.25*	✕
	2	60 *0.3*	80 *0.4*	100 *0.5*	120 *0.6*	140 *0.7*	160 *0.8*	5 (fixed) *0.025*				0.5 *0.0125*	1 *0.25*	✕
	3	60 *0.3*	80 *0.4*	100 *0.5*	120 *0.6*	140 *0.7*	160 *0.8*	5 *0.025*	10 *0.05*	15 *0.075*	20 *0.1*	1 *0.25*		✕

The 3D simulations are then conducted under the previously investigated four mechanical BC of the damaged hybrid composite beams and two electric conditions on the patches electrodes. It's worth noticing that, for the ISL damage model, the number and thickness of Teflon® layers vary in terms of the damage geometric characteristics. Due to the space limitation, only the first mode CF BC related SC squared FCF results, for normalized damages characteristics (X_d/L, L_d/L, H_d/H), are shown for the RM and ISL in Fig. 5. The latter indicates that: (i) for all parametric analysis cases, RM damage is much more influential on the SC FCF indicator than does the ISL one; (ii) for a fixed damage position (case 1), SC FCF indicator increases for both damages when increasing the latters' length and height, but more rapidly for the former than for the latter; (iii) for fixed damage length (case 2) and thickness (case 3), SC FCF indicator behaves oppositely for RM and ISL damages when varying the damages positions; it is higher for RM at the beam root, while it is lower for ISL at this position.

Maximum reached squared FCF values for both damages' models, four BC and two electric conditions are summarized in Table 6. It can be noticed that: (i) RM induced squared FCF is much higher than ISL one; (ii) maximum values are obtained for the CF BC for both damage models but with different values and for different modes and damages characteristics; SC and OC squared FCF reach the same maximum values and for the same modes, except for ISL under CF.
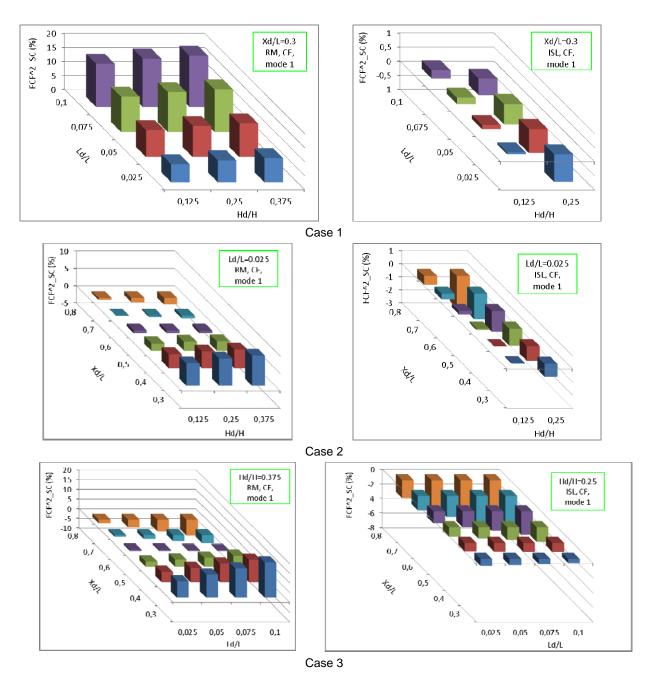
Case 1

Case 2

Case 3

Fig. 5 SC squared FCF parametric analysis for *mode 1* of *CF* hybrid composite beams

Table 6 Damage characteristics of maximum reached squared FCF indicators

Damage	Indicator	Characteristics	CF	CS	CC	SS
RM	SC	[X_d, L_d, H_d]	[**140** 20 1.5]	[100 20 1.5]	[100 20 1.5]	[100 20 1.5]
		(%, mode)	(**24.04**; **6**)	(19.08; 6)	(20.64; 6)	(20.07; 6)
	OC	[X_d, L_d, H_d]	[140 20 1.5]	[100 20 1.5]	[100 20 1.5]	[100 20 1.5]
		(%, mode)	(**24.04**; **6**)	(19.08; 6)	(20.64; 6)	(20.07; 6)
ISL	SC	[X_d, L_d, H_d]	[**160** 20 1]	[120 20 1]	[100 20 1]	[100 20 1]
		(%, mode)	(**-7.02; 3**)	(-6.26; 4)	(-6.58; 4)	(-5.28; 3)
	OC	[X_d, L_d, H_d]	[160 20 1]	[120 20 1]	[100 20 1]	[100 20 1]
		(%, mode)	(-6.54; 1)	(-6.27; 4)	(**-6.58**; **4**)	(-5.28; 3)

4. CONCLUSIONS

This contribution presented short-circuit (SC) and open-circuit (OC) simple and squared frequency change factors (FCF) for the damage detection in hybrid laminated composite beams using piezoceramic patches integrated in a symmetrical configuration. The structural damage was modeled using removal of material (RM), simulating a notch or crack, and inclusion of soft layer (ISL), simulation a delamination The proposed damage indicators performance analysis was investigated using three-dimensional fully coupled piezoelectric finite elements (FE) under four mechanical boundary conditions and for varying damage geometric characteristics (position, length and height). It was found that the squared FCF are much more performant than the classical simple ones; also, both damage indicators were found to be much more influenced by varying the RM model characteristics than the ISL ones; besides, it was shown that the popular numerical cantilever and analytical simple support boundary conditions (BC) are not suitable for investigating theoretically frequency-based RM damage detection since in these cases, changes of modes order and type occur, rendering the obtained results specific and not generalizable to other BC; it is then recommended for numerical analysis, to prefer clamped-clamped BC for these and for practical reasons. As an extension of the present work, modal energy-based damage indicators have been explored; for space limitation, corresponding results will be presented separately.

ACKNOWLEDGMENTS

REFERENCES

Al-Ajmi, M.A. and Benjeddou, A. (2008), "Damage indication in smart structures using modal effective electromechanical coupling coefficients". *Smart Mater. Struct.*, **17**(3), art. n° 035023 (15 pages).

Benjeddou, A. (2006), "First use of the shear piezoceramics and effective electromechanical coupling coefficient for damage detection and characterization", *Proceedings of 3rd European Workshop on Structural Health Monitoring*, Granada.

Benjeddou, A., Vijayakumar, S. and Tawfiq, I. (2006), "A new damage identification and quantification indicator for piezoelectric advanced composites, *Proceedings of the 3rd ECCM on Solids. Structures and Coupled Problems in Engineering*, Lisbon.

Giurgiutiu, V., Lin, B., Santonni-Bottai, G. and Cuc, A. (2011), "Space application of piezoelectric wafer sensors for structural health monitoring", *J. Intell. Mater. Syst. Struct.*, **22**(8), 1359-1370.

Huang, G., Song, F. and Wang, X. (2010), "Quantitative modeling of coupled piezo-elasto-dynamic behavior of piezoelectric actuators bonded to an elastic medium for structural health monitoring: a review", *Sensors,* **10**, 3681-3702.

Ihn, J.B. and Chang, F.K. (2008), "Pitch-catch active sensing methods in structural health monitoring for aircraft structures", *Struct. Health Monit.*, **7**(1), 5-19.

Jian, X.H., Tzou, H.S., Lissenden, C.J. and Penn, L.S. (1997), "Damage detection by piezoelectric patches in a free vibration method", *J. Compos. Mater.*, **31**(4), 345-359.

Penn, L.S., Jump, J.R. and Geenfield, M.J. (1999), "Use of free vibration spectrum to detect delamination in thick composites", *J. Compos. Mater.*, **33**(1), 54-72.

Qian. P., Lestari. W., Shah, M.G. and Wang, J. (2007), "Dynamics-based damage detection of composite laminated beams using contact and non-contact measurement systems", *J. Compos. Mater.*, **41**(10), 1217-1252.

Sinou, J.J. (2009), "A review of damage detection and health monitoring of mechanical systems from changes in the measurements of linear and nonlinear vibrations", In Sapri R.C, (Ed.), *Mechanical vibrations: measurement, effects and control*, Nova Sci. Pub., Chap. 13, 643-702.

Tan, P. and Tong, L. (2004), "Delamination detection of composite beams using piezoelectric sensors with evenly distributed electrode strips", *J. Compos. Mater.*, **38**(4), 321-352.

Yam, L.H., Wei, Z. and Cheng, L. (2004), "Nondestructive detection of internal delamination by vibration-based method for composite plates", *J. Compos. Mater.*, **38**(24), 2183-2198.

APPENDIX A

Table 7 Materials properties

Elastic	E_1 (GPa)	E_2 (GPa)	E_3 (GPa)	G_{12} (GPa)	G_{13} (GPa)	G_{23} (GPa)	ν_{12}	ν_{13}	ν_{23}
CFRP (M55J/914)	270	5.54	5.54	3.87	3.87	8	0.36	0.36	0.45
GFRP (G837/914)	80.6	80.9	80.9	5.1	5.1	11	0.3	0.3	0.45
Teflon®	1.6	1.6	1.6	0.6	0.6	0.6	0.35	0.35	0.35
PZT-5A	61	61	53.2	22.59	21.1	21.1	0.35	0.35	0.38
Piezoelectric	e_{31} (C/m^2)	e_{32} (C/m^2)	e_{33} (C/m^2)	e_{15} (C/m^2)	e_{24} (C/m^2)	$\dfrac{\in_{11}^s}{\in_0}$	$\dfrac{\in_{22}^s}{\in_0}$	$\dfrac{\in_{33}^s}{\in_0}$	$\in_0$ (pF/m)
PZT-5A	-7.21	-7.21	15.11	12.32	12.32	915	915	777	8.854